PCCP

Accepted Manuscript

ROYAL SOCIETY OF CHEMISTRY

www.rsc.org/pccp

Unexpectedly large impact of van der Waals interactions on the description of heterogeneous catalyzed reactions: the water gas shift reaction on Cu(321) as a case example

Héctor Prats, Pablo Gamallo, Ramón Sayós, Francesc Illas

Departament de Química Física & Institut de Química Teòrica i Computacional (IQTCUB), Universitat de Barcelona, C/Martí i Franquès 1, 08028 Barcelona, Spain.

Abstract.

The molecular mechanisms of the water gas shift reaction on Cu(321) have been chosen to investigate the effect of dispersion terms on the description of the energy profile and reaction rates. The present study based on periodic DFT calculations shows that including dispersion terms does not change the qualitative picture of the overall reaction, maintaining the rate determining step and the predominant route. However, the effect of dispersion is different for different adsorbates —reactants, intermediates or products— with a clear net effect and with no compensation of errors. Thus, in the OH+OH $\rightarrow H_2O+O$ process the dispersion effects imply up to three orders of magnitude in the calculated reaction rates; the formation of carboxyl is highly disfavoured when dispersion terms are explicitly included and finally, the reaction rate for CO_2 production (at 463 K) through *cis*-COOH dissociation is enhanced by three orders of magnitude by including dispersion terms in the calculation of the energy barrier. Consequently, the inclusion of dispersion terms largely affects the overall potential energy profile and produces tremendous changes in the predicted reaction rates. Therefore, dispersion terms must be included when aiming at obtaining information from macroscopic simulations employing for instance microkinetic or kinetic Monte Carlo approaches, where these effects should be clearly shown.

Introduction

Density functional theory (DFT) based calculations carried out on suitable periodic surface models have enormously contributed to our understanding of heterogeneously catalyzed reactions at the molecular level to the point that they have nowadays become a rather standard tool as illustrated in recently published books.[1,2] This type of computational methodology allowed to take into account environmental effects into the equilibrium structure of surfaces exposed to gases,[3] determining rather accurate energy profiles for many heterogeneously catalyzed reactions thus unveiling the molecular mechanism behind complex processes involving many elementary steps [4] and helped to derive useful concepts as descriptors allowing for a rational design of potential new and improved catalysts.[5,6] The information extracted from the DFT based calculations often includes transition state theory (TST) reaction rate constants for the elementary steps which can be used in subsequent macroscopic simulations of complex reactions. For instance the microkinetic modeling[7] of the water gas shift reaction (WGSR) catalyzed by Cu(111) by Gokhale et al.[8] and the kinetic Monte Carlo simulations by Yang et al.[9] and Prats et al.,[10] both based on DFT calculated rates, constitute an excellent example of the interpretative and predictive power of this computational approach. Moreover, the increasing use of models involving stepped surfaces[11-16] or large metallic nanoparticles [17] provides more realistic models of the catalytic active sites. Yet, one of the remaining problems in this field concerns the accuracy of the calculated total energy defining the potential energy surface. In fact, commonly used Generalized Gradient Approach[18,19] (GGA) forms of the exchange-correlation potential such as PW91[20] or PBE[21] provide a balanced and rather accurate description of the bulk properties of the three series of transition metals whereas other broadly used functionals such as RPBE exhibit a poorer behavior and excessively stabilize surface energies.[22,23] Nevertheless, these GGA functionals do not provide accurate enough results for main group elements containing molecules[24] and, as already pointed out by Kristyan and Pulay twenty years ago,[25] neglect dispersion terms which may play a non-negligible role in the molecular picture of heterogeneously catalyzed reactions.

The first of the two shortcomings of DFT mentioned above has precisely triggered the development of new and more accurate functionals such as the widely used B3LYP hybrid functional [26] or the series of Minnesota hybrid meta-GGA functionals.[27-29] These

are, however, seldom used in computational studies in heterogeneous catalysis due to the difficulty that these methods face when applied to metals.[30-,32] Because of their good performance, hybrid functionals are surely the most popular kind of functionals in molecular chemistry and homogeneous catalysis.[33] However, for extended systems they have large, and often excessive, computational demands as compared to GGA type functionals. This is due to the long range of the exchange interactions when making use of programs working in the real space and due to the requirement for dense Brillouin zone sampling when relying on programs using plane wave basis sets.[34] Nevertheless, it is often argued that, for chemical reactions taking place at metal surfaces, calculated relative energies are much less affected than absolute energies by the inherent errors of GGA type functionals[2,4,35,36] and this is surely one of the keys of the success of this type of calculations.

The effect of van der Waals (also known as dispersion) interactions on adsorption properties has been the focus of an intense research in the past few years, especially after the landmark contributions of Grimme and coworkers,[37-39] which has triggered many new theoretical developments and the appearance of a plethora of new functionals aiming to account for these terms in an accurate and non-empirical way as recently critically reviewed by Klimes and Michaelides.[40] Dispersion terms play an important role in chemical and physical processes involving biomolecules and their role in conformational related problems and in thermochemistry has been recently reviewed.[41] These terms largely affect the adsorption properties of molecules at surfaces and can even be the dominant term as in the case of aromatic molecules interaction with the basal plane of MoS_2,[42] hydrocarbons interacting with zeolites [43] or graphene on metallic surfaces;[44] a review on the role of dispersion terms on adsorption properties has been recently published.[45]

In spite of the large number of articles devoted to study the importance of dispersion terms in adsorbate-surface interactions, there is almost no information regarding the effect of dispersion terms in the energy profile of heterogeneously catalyzed reactions, especially for complex mechanisms involving several elementary steps. An important catalyzed reaction with special technological relevance[46] is the WGSR transforming CO and H_2O into CO_2 and H_2. This process takes place in two stages, at high and low temperature, respectively. The catalyst for the low temperature stage involves Cu nanoparticles

supported on different oxides[47] although other metals and supports have also been proposed.[48,49] The molecular mechanism for the low temperature catalyzed WGSR involves a rather large number of elementary steps and two possible routes, redox or carboxyl, are possible.[8] These have been studied in depth for the Cu(111)[8] and Cu(321)[13] surfaces; the latter one, containing different low-coordinated sites, offers a more realistic model of the catalyst. Moreover in the latter case, there is detailed information regarding the structure of the many transition state structures involved in the mechanism and thus constitutes an excellent system to check the effect of the dispersion terms on the overall energy profile and rate constants. This is precisely the goal of the present paper. We will provide compelling evidence that while the qualitative picture of the overall reaction scheme is not largely affected by the inclusion of the dispersion terms, there are significant differences in the calculated reaction rates, which have important implications in the macroscopic description of the overall process via microkinetic or kinetic Monte Carlo simulations.

Elementary steps in the water gas shift reaction

In this section we will briefly summarize the most salient features of the reaction mechanisms proposed for the WGSR. These can be grouped in two general mechanisms, namely redox and associative, although with at least two variants in each route. Both mechanisms share the first three elementary steps, which correspond to CO and H_2O adsorption and subsequent dissociation of adsorbed H_2O into adsorbed H and OH, and also share formation of adsorbed H_2 through recombination of H adsorbed atoms and, eventually, subsequent desorption of adsorbed H_2 and CO_2 products. However, there are notable differences in the formation of adsorbed CO_2. Hereafter, we will assume that any reaction species is in the adsorbed state omitting the usual convention to denote any adsorbed A species as A*. To avoid confusion, any B species in the gas phase will be explicitly denoted as B(g).

The two possible variants along the redox route are direct hydroxyl dissociation ($OH \rightarrow O + H$) and hydroxyl disproportionation ($OH + OH \rightarrow O + H_2O$) although both involve CO_2 formation through direct reaction between adsorbed CO and O ($CO + O \rightarrow CO_2$). Hence, the two variants differ in the way O is produced. On the other hand, the associative mechanism is based on the formation of a carboxyl intermediate following CO

+ OH → COOH. The decomposition of this intermediate yields CO_2 either through direct dehydrogenation (COOH → CO_2 + H) or assisted dehydrogenation (COOH + OH → CO_2+ H_2O). In addition, monodentate and bidentate formate (HCOO) species are also possible reaction intermediates. These species are formed by CO_2 hydrogenation but have solely a spectator role.

The study of Fajín et al.[13] evidenced that the presence of steps increases the water adsorption energy and decreases the energy barrier of water dissociation and atomic hydrogen recombination steps which on Cu(321) are found to constitute the rate-determining steps (rds). Interestingly, these two elementary steps are also the rds for the WGSR on Cu(111) but on the stepped Cu(321) they have similar energy barriers and reaction rates while on the flat Cu(111) surface the water dissociation has an energy barrier considerably larger than the hydrogen recombination.

In the present work, the effect of van der Waals interactions will be explicitly taken into account for all adsorption, reaction and desorption steps outlined above using Cu(321) as catalyst model as described in the next section.

Surface model and computational details

The interaction of the different reactants, intermediates and products involved in the WGSR catalysed by the Cu(321) surface has been obtained from periodic DFT calculations modelled through the usual repeated slab approach with a 2×2×1 supercell constructed using the optimum lattice parameter of 3.63 Å for the computational method chosen here and described in detail below; note that this is sufficiently close to the experimental value of 3.62 Å.[50] It is also worth pointing out that, in order to minimize lateral interactions, the unit cell for the Cu(321) slab model thus defined is larger than the one previously used by Fajín et al.[13] The 2×2×1 supercell used in the present work contains 60 Cu atoms distributed in four atomic layers as schematically shown in Figure 1 and consists of a monoclinic prism with an angle of 104.96º between the x and y axes and of 90º for the angles between x and z or y and z axes. Further, the unit cell vectors along the x, y and z directions have different lengths. The corresponding fractional coordinates of the atoms in this unit cell were obtained using the Materials Studio computer code (version 8.0).[51] The unit cell for the two-dimensional slab thus obtained was modified by adding a vacuum

region of 12 Å and scaling the fractional coordinates conveniently so as to obtain a unit cell that can be replicated in three dimensions as required when using a plane-wave periodic DFT approach. The resulting slab was further modified by allowing full relaxation of the position of the uppermost 28 Cu atoms within the computational approach described below.

In order to investigate the impact of the dispersion terms in the calculated energy profile we compare results from two series of periodic DFT calculations, both carried out with the VASP code.[52-54] For the first series we rely on the PW91 calculation of Fajín et al.[13] whereas in the second one the effect of the van der Waals interactions has been included by adding the dispersion term obtained from the D2 method of Grimme [38] to the PBE calculated energy (PBE-D2). Note in passing by that, in spite of its semiempirical flavor, the D2 method has been shown to properly describe the physisorption and chemisorption states of graphene with Ni(111).[44] Nevertheless, to validate the present results some key calculations have been carried out with the D3 parameterization of Grimme[39] (PBE-D3) and with the more physically grounded method proposed by Tkatchenko et al.[55] (DFT-T). Note also that PW91 and PBE results for bulk properties of transition metals[22,23] and also for the description of the adsorption energy of WGSR species are very similar.[56]

The valence electron density was expanded in a plane-wave basis set with a cut-off of 415 eV for the kinetic energy. The effect of core electrons in the valence electron density was taken into account through the projector augmented wave (PAW) method [57] as implemented in VASP.[58] Numerical integration in the reciprocal space was carried out by employing a 5×5×1 Monkhorst-Pack grid of special k-points.[59] The energy cut-off and k-point grid values were chosen after a systematic study of the geometry and energy convergence. Spin polarization is taken into account whenever species with possible radical character are involved even if, as shown by Fajín and coworkers,[60] the open-shell character is likely to be quenched by the metallic character of the substrate.

The geometry optimization calculations carried out to locate the most stable structure of adsorbed species started from the structures reported by Fajín et al.,[13] the positions of the ions and the nearest surface Cu atoms (defined as those having distances to adsorbate atoms lesser than 3 Å) were relaxed using the conjugate-gradient algorithm. The

convergence thresholds were 10^{-6} eV for the total energy and 10^{-3} eV/ Å for the forces acting on the cores. The transition states for the different elementary steps were determined with the improved Dimer method by Heyden et al. [61] with the same relaxation criteria. A proper frequency analysis indicating the presence of single imaginary frequencies ensured that the structures located with the Dimer method correspond to true transition states. Adsorption energies, co-adsorption energies, and energy barriers have been corrected for the zero-point vibrational energy (ZPE) within the harmonic oscillator approximation and, therefore, the subsequent presentation and discussion of results consider always ZPE-corrected energies.

The adsorption energies (E_{ads}) for all the isolated species on the slab surface model have been calculated as

$$E_{ads} = E_{slab-m} - E_{slab} - E_m \quad (1)$$

where E_{slab-m} and E_{slab} refer to the total energy of the slab model representing the Cu(321) surface with and without the m adsorbate and E_m corresponds to the total energy of the molecule in the gas phase computed, as usual, by placing it in a box with the same size of the unit cell for the slab. For the situations with two adsorbates above the surface unit cell the co-adsorption energy is calculated as:

$$E_{coad} = E_{slab-m1-m2} - E_{slab} - E_{m1} - E_{m2} \quad (2)$$

where $E_{slab-m1-m2}$ stands for the total energy of the system formed by the two species adsorbed on the slab and E_{slab}, E_{m1} and E_{m2} are as in Eq. (1).

Results and discussion

Adsorption and co-adsorption of reactants, intermediates and products

In this subsection we discuss the effect of dispersion on the most favourable adsorption and co-adsorption configurations of the species involved in the WGSR mechanism catalysed by the Cu(321) surface. A summary of calculated results regarding adsorption energy is reported in Tables 1 and 2 whereas Figure 2 and Figure 3 report the equilibrium geometry of the adsorbed and co-adsorbed states for all involved species, respectively.

In agreement with the previous study of Fajín et al.,[13] water prefers to be adsorbed in the step region with the O atom linked to the Cu(1) surface atom and the two H atoms pointing to the lower terrace. The PBE-D2 adsorption energy for this configuration is -0.66 eV, which is very close to the PW91 result for the same surface (-0.58 eV) and 3-4 times larger than the reported value for the flat Cu(111) surface (-0.18 eV),[8] confirming the importance of the low-coordinated Cu atoms in the stabilization of the adsorbates. For adsorbed CO, the most stable configuration is also in the step region with a PBE-D2 calculated E_{ads} of -1.11 eV, again in very good agreement with the PW91 result of Fajín et al. (-0.95 eV) and twice larger than in the Cu(111) surface (-0.51 eV).[8] For the OH and COOH intermediates the PBE-D2 values are again very close to the PW91 ones and significantly larger than for the Cu(111) surface. Note that both intermediates are more stable when adsorbed on the bridge sites between Cu(1) and Cu(2) atoms (Figure 2b and 2d) and that while the OH intermediate is clearly more stable in this stepped surface (-3.35 eV versus -2.77 eV for the Cu(111) surface), the adsorption energy for the COOH adsorbate is only 0.20 eV larger. Finally, both reaction products, CO_2 and H_2, interact weakly with the Cu(321) surface with PBE-D2 E_{ads} values of -0.28 and -0.12 eV only. It is worth pointing out that on the flat Cu(111) the CO_2 adsorption energy is even lower (-0.09 eV) and H_2 does not adsorb at all.[8] However, a close inspection to Table 1 shows that while the PW91 and PBE-D2 E_{ads} values for H_2O, OH, CO, COOH and H_2 are very similar, a significant difference is found for CO_2. In fact, the inclusion of the van der Waals interactions through the D2 method of Grimme[37] has a strong effect on the adsorption energy of the CO_2 molecule; the PW91 value reported by Fajín et al.[13] is of -0.06 eV only, much lower than the present PBE-D2 value. In order to validate the present result and to exclude a possible artefact of the D2 parameterization two other vdW corrections, namely D3[39]and Tkatchenko et al.[55] methods, have been used giving E_{ads} values of -0.22 and -0.32 eV, respectively, in agreement with the D2 method (see also discussion at the end of the results section). Cleary, neither PBE nor PW91 functionals can properly describe the physisorption of the quite stable CO_2 molecule and vdW corrections should be included. This effect is also observed for CO molecule, although to a lesser extent: from -0.95 to -1.11 eV. Note that this discrepancy does not come from the change in the functional because, as already discussed, PBE and PW91 essentially provide similar results. Hence,

the worst possible scenario emerges where dispersion does not affect all species in a similar way.

Co-adsorption energies of the most stable configuration of reactant and product pairs for the different elementary steps in the WGSR mechanism are listed in Table 2 and the corresponding geometries are shown in Figure 3. All co-adsorption energies involving radicals have been obtained from spin polarized calculations for all the possible spin arrangements approaching multiplet (singlet, doublet, triplet…) states and the results show that for an even total number of electrons (H+H, OH+H, CO+O…) the most stable state is the global closed shell singlet, although the energy differences with the first most stable triplet state are only of the order of ~0.05 eV. Analysing the most stable adsorption sites for the different adsorbate pairs (Figure 3) one can readily see that the atomic species (H and O) are typically found in the threefold-coordinated hollow sites, whereas OH prefers the bridge sites, and finally CO and the largest adsorbates are usually found in the step region, again evidencing the importance of the low-coordinated Cu atoms in the stabilization of the adsorbates. Results in Table 2 also evidence that the effect of dispersion is different for different adsorbate pairs which, as we will show in the next sections, must have an influence on several energy barriers and on the resulting TST reaction rates. In fact, the effect is almost negligible (~ 0.05 eV) for some cases such as OH_a+H_b, O+H, or H_a+H_b, it is intermediate (<0.15 eV) for some others such as OH_a+OH_b or CO_a+O_b and quite large (>0.25 eV) in a few cases such as CO_a+OH_b or CO_2+H. The differences are large enough to be significant and likely to be present if other methods are used to estimate the dispersion contribution to the total energy.

Energy barriers of the elementary steps

Now we come to the most important part of the present work, namely the description of the calculated energy barriers for the different elementary steps in the WGSR on Cu(321). The energy barrier for each individual step of the reaction mechanism has been calculated as the energy difference between the transition state, located using the improved Dimer method [61] and that of the most stable adsorption (or co-adsorption) configuration for the reactant(s). For the transition state (TS) calculations, a first step involved the search of a first order saddle point with the slab structure fixed and, in a second step, the atoms in the

slab uppermost layers were allowed to relax out to refine the geometry and quantify the effect of the surface relaxation in the calculated energy barriers. ZPE corrected values, for the energy barriers obtained from PBE-D2 in the forward and reverse directions are given in Table 3 where equivalent ZPE corrected PW91 values have been included for comparison. Schematic representations of the transition state geometries are given in Figure 4. For products desorption (i.e., $H_2 \rightarrow H_{2(g)}$ and $CO_2 \rightarrow CO_{2(g)}$) the TSs are assumed to be their final states, that is, H_2 and CO_2 in the gas phase. Thus, the energy barriers for these processes are equal to their adsorption energies in absolute value (i.e., 0.12 and 0.28 eV, respectively) and, consequently, are not included in Table 3. In the following we will discuss the effect of dispersion in the different steps by comparing to the results reported by Fajín et al. [13] with appropriate comparison to the results reported for Cu(111) not including dispersion terms [8] whenever needed. Hence, the appropriate comparison involves the different steps on the Cu(321) with and without dispersion or on the Cu(321) and Cu(111) surfaces both without dispersion terms included.

Water dissociation. This step is endoergic by 0.20 eV with an energy barrier of 0.78 eV (Table 3), significantly lower than the 1.01 eV value for Cu(111) surface, and very similar to the ZPE corrected PW91 value obtained by Fajín of 0.71 eV. To further validate the present result, the energy barrier corresponding to this step has been calculated also including the vdW interactions through the DFT-T method obtaining a value of 0.79 eV, in very good agreement with the PBE-D2 results. Here including the vdW correction has a minor effect. It is worth pointing out that the lower energy barrier for this surface implies a greater reaction rate for water dissociation and hence, in principle, a concomitant enhancement of the reactivity towards WGSR. However, the reaction rate for the reverse process has been increased even more, because, while here the reaction is endoergic, in the flat Cu(111) surface this step is practically isoergic (ΔE = 0.01 eV). Therefore, the reactivity depends on whether forward reaction rates of the other processes can compete with the water formation.

OH dissociation. This step is endoergic by 0.48 eV, almost the same value than for Cu(111) surface, and has an energy barrier of 1.51 eV (Table 3), higher than for the flat surface (1.19 eV) [8] and, as the previous step, very similar to the value obtained without including vdW corrections (1.55 eV).[13] The high energy barrier for this reaction implies that the CO_2

formation via the redox mechanism through direct OH dissociation in the Cu(321) surface will surely be the least frequent route among all.

OH disproportionation. This is an alternative path for producing atomic oxygen, it is exoergic by -0.10 eV with an energy barrier of only 0.46 eV, becoming the main route of redox mechanism. Surprisingly, this value is increased by 0.32 eV when vdW interactions are not considered (Table 3).

CO oxidation by atomic O. This step is exoergic by -0.48 eV, a value significantly different than in the Cu(111) surface (-0.78 eV). The PBE-D2 energy barrier for this process is 0.68 eV almost the same as obtained from PW91 (0.60 eV) even if the latter does not include the effect of dispersion. The high exoergicity of this process implies that the reverse direction is hardly to happen.

Carboxyl formation through CO oxidation by OH. Direct CO oxidation by OH to produce surface carboxyl species represents a viable alternative to the previous step, with a PBE-D2 energy barrier of 0.84 eV, slightly higher than the value reported for the Cu(111) surface (i.e., 0.70 eV). In the flat surface this process is endoergic by only 0.15 eV, the endoergicity is heavily increased in the Cu(321) surface. Note that this value is also different from the value reported by Fajín et al. [13] (0.22 eV), where the energy barrier reported was of 0.46 eV. The reason of this difference is that the CO+OH pair is significantly stabilized by inclusion of vdW interactions (Table 2).

Carboxyl dehydrogenation. This is an exoergic step (-0.52 eV) with an energy barrier of 0.80 eV (Table 3), again significantly lower than for the flat Cu(111) surface (1.18 eV) and also lower that the PW91 value obtained (1.10 eV).[13] Since the inclusion of vdW interactions stabilizes both the transition state and the final products, CO_2 formation through carboxyl intermediate will probably play a more important role in the WGSR over Cu(321) than in Cu(111).

Carboxyl disproportionation by hydroxyl. This step involving cis-COOH is also exoergic by -0.64 eV, more than for the Cu(111) surface (-0.37 eV). The energy barrier for this process is 0.33 eV to be compared to 0.55 eV without vdW correction, which in turn needs to be compared with the result obtained for the flat surface (0.38 eV).

H recombination. This step is common to the four investigated routes. According to the present result, H atoms are not provided only by water dissociation but also by carboxyl dehydrogenation. Another possible process for H production is OH dissociation which is very unfavourable even in this stepped surface. Although H_2 does not adsorb molecularly on Cu(111) it does on the Cu(321) surface by -0.12 eV (see Table 1). This reaction is endoergic by 0.31 eV, with an energy barrier of 0.78 eV, again smaller than the ZPE corrected 0.96 eV value for the Cu(111) surface.

Reaction rates of the elementary steps

From the calculated zero point corrected energy barriers and vibrational frequencies one can readily obtain the corresponding transition state theory rates at the temperature of interest. Table 3 reports the calculated rates for the elementary steps at 463 K; this is the same temperature used in previous work regarding the WGSR mechanism on the Cu(111) [8] and Cu(321) [13] surfaces, where dispersion terms were not included in the calculations.

As discussed above and in agreement with Fajín et al.,[13] the presence of low-coordinated Cu atoms plays an important role in the stabilization of the reactants, with adsorption energies twice or even three times larger than in the flat Cu(111) surface but with significant differences in the results corresponding to the Cu(321) surface depending on whether dispersion terms are neglected or included. Nevertheless, the difference to Cu(111) is very large, implying a reduction of seven and five orders of magnitude for the reaction rates of CO and H_2O desorption at T = 463K, respectively. This is likely to be due the coverage of these species leading to higher H_2 productions although macroscopic simulations are needed to further check if this strong stabilization of reactants enhances the reactivity.

The dissociation of adsorbed water defines the rds in all cases and all results seem to indicate that the associative mechanism is clearly preferred. Nevertheless, the rates predicted by the present PBE-D2 calculations for the rds are one order of magnitude smaller than the values reported from PW91 not including dispersion terms. Here it is worth to mention that the low energy barrier for the reverse process leads to a reaction rate of $6.38 \cdot 10^6$ s^{-1}, six orders of magnitude larger than in the flat surface ($5.25 \cdot 10^0$ s^{-1}) and greater than the rate for the forward process. Clearly, it is not possible to extract reliable

conclusions from the energy barrier for the rate-determining step in the forward direction only.

Results in Table 3 show that the effect of dispersion on all elementary steps is very different. In some cases including or not these effects has a variation of barely one order of magnitude in the calculated rates for the forward reactions. This is for instance the case of $H_2O \rightarrow OH+H$, $OH \rightarrow O+H$, $CO+O \rightarrow CO_2$, *cis*-COOH+OH $\rightarrow CO_2 + H_2O$, and $H+H \rightarrow H_2$ steps. However, in some other steps the effect of dispersion implies up to three orders of magnitude in the calculated reaction rates, as this is the case for $OH+OH \rightarrow H_2O+O$, which now appears as the dominant source of adsorbed O. This is especially relevant since including dispersion affects the reaction rate of the main step in CO_2 production also by three orders of magnitude but in the opposite sense. The formation of carboxyl is highly disfavoured when dispersion terms are explicitly included. The reaction rate for CO_2 production (at 463 K) through *cis*-COOH dissociation is enhanced by three orders of magnitude by including dispersion terms in the calculation of the energy barrier. Finally, it is worth to mention that, not surprisingly, dispersion terms largely affect the reaction rates for adsorption and desorption steps (not reported).

At this point, one may still argue that semiempirical dispersion treatments based on atom pairwise potentials may be inadequate for metallic systems and question the overall validity of the present results. The selected adsorption energy values reported above calculated using the D3 and Tatchenko methods would indicate that this is not the case. Nevertheless, to reach a firm conclusion it is convenient to inspect energy barriers as well. To this end, a new series of calculations has been carried out using the method recently proposed by Andersson consisting in a clever yet simple modification of the DFT-D2 method of Grimme which provides good results in metallic systems.[62] This method takes into account screening of the dispersion forces by the conducting valence electrons in the metal, includes the main physics and reproduces a wide variety of experimental data for both bulk metallic systems as well as adsorption onto metal surfaces. The main idea is to introduce a hard cutoff to the dispersion interaction and to conveniently replace the C_6 coefficients for metal atoms. Using this approach, all adsorption energies for reactants and products and energy barriers for two of the most important elementary steps (i.e. $H_2O \rightarrow OH+H$ and $CO+O \rightarrow CO_2$) have been calculated. The ZPE corrected adsorption energy

values of CO, H_2O, CO_2 and H_2 calculated in this way (-1.03, -0.57, -0.19 and -0.08 eV, respectively) are very close to the PBE-D2 values in Table 2 to the point that the changes are within the incertitude of DFT methods. The equilibrium geometries calculated with PBE-D2 and PBE-Anderson methods are almost the same and the calculated surface reaction energy barriers differ in less than 0.05 eV. Consequently, one can firmly claim that the conclusion arising from the PBE-D2 calculations reported in the present work are physically meaningful.

Conclusions

The effect of dispersion terms on the description of the energy profile and reaction rates of a complex heterogeneously catalysed process has been studied in detail taking the water gas shift reaction on Cu(321) as a case example. This is a convenient case study because a rather large number of elementary steps and because of the existence of previous results regarding the molecular mechanism of the overall reaction on this surface [13] and in the flat Cu(111) surface [8], but both neglecting dispersion effects.

Including dispersion terms does not change the qualitative picture of the overall reaction; the rate determined step and the predominant route are not affected by including or neglecting these terms. However, the present results show that, in spite of the rather small size of the species involved in the molecular mechanism of the WGSR, the contribution of dispersion to the overall picture is important and should not be ignored. The effect of dispersion is different for several adsorbates —reactants, intermediates or products— with a clear net effect and with no compensation of errors. Dispersion terms affect adsorption structures and adsorption energies but also contribute to determine the transition state and the energy barriers with differential effects on final forward and reverse values of up to 0.4 eV. This seemingly small value has a huge effect on the transition state theory computed reaction rates.

One must admit that the present results have been obtained from a particular choice in the method used to estimate dispersion terms. Nevertheless, calculations for the key steps have been also carried out including dispersion with two alternative methods indicating that the conclusions of the present work are sound and not biased.

To summarize, while the inclusion of dispersion terms does not change the qualitative description of the WGSR catalysed by Cu(321), their presence largely affects the overall potential energy profile and produces tremendous changes in the predicted reaction rates. Consequently, dispersion terms must be included when aiming at obtaining information from macroscopic simulations employing for instance microkinetic or kinetic Monte Carlo approaches, where these effects should be clearly shown.

Acknowledgements

Financial support to this research has been provided by the Spanish MINECO CTQ2012-30751 and CTQ2014-53987-R grants and, in part, from the *Generalitat de Catalunya* grants 2014SGR97, 2014SGR1582 and XRQTC. HPG thanks *Generalitat de Catalunya* for a predoctoral FI-DGR-2015 grant. Computational resources provided by *Consorci de Serveis Universitaris de Catalunya* (CSUC, former CESCA) are gratefully acknowledged.

Table 1.- Adsorption energies for the adsorption of the WGSR species on Cu(321) as predicted from PBE-D2 and PW91 calculations. The different adsorption sites are indicated with numbers referring to the labels in Figure 1 and with b indicating bridge sites. All values are in eV and ZPE corrected.

Species	**Adsorption site**	**PBE-D2**	**PW91**[13]
H_2O	top1-step	-0.66	-0.58
OH	$b_{2\text{-}1}$	-3.35	-3.40
CO	top1	-1.11	-0.95
COOH	$b_{2\text{-}1}$	-2.05	-1.95
CO_2	top1-step	-0.28	-0.06
H_2	top1	-0.12	-0.12

Table 2.- Co-adsorption energies for the adsorption of the WGSR species on Cu(321) as predicted from PBE-D2 and PW91 calculations. Sites are defines as in Table 1. All values are in eV and ZPE corrected.

Species	**Adsorption sites**	**PBE-D2**	**PW91**
OH_a+H_b	b_{4-1} / hole "a"	-5.51	-5.47
CO_a+OH_b	top1 / hole "a"	-4.43	-4.05
OH_a+OH_b	b_{2-1}/b_{3-1}	-6.28	-6.40
O+H	hole "a" / b_{4-1}	-7.35	-7.31
CO_a+O_b	top1 / hole "a"	-5.91	-5.84
$H_2O_a+O_b$	top1-step / hole "b"	-5.82	-5.67
H_a+H_b	hole "a"/ hole "f	-4.77	-4.81
$CO_aO_bH+O_cH$	b_{2-1} / top4	-5.20	----
CO_2+H	top1-step / hole "b"	-2.72	-2.47
$CO_2+H_2O_a$	b_{2-4} / top1-step	-0.91	-0.70

Table 3.- Elementary steps characterization of the WGSR on the Cu(321) surface: imaginary frequencies associated to the transition state structure (ν_i in cm^{-1}), ZPE corrected energy barriers (E_b in eV) and reaction rates at 463 K (r in s^{-1}) for the forward and reverse reactions of the elementary steps as predicted from PBE-D2 calculations. ZPE corrected PW91 values from Fajín et al.[13] for the forward reaction are given in parenthesis for comparison.

Elementary step		**Forward**		**reverse**	
	ν_i	**E_b**	**r**	**E_b**	**r**
$H_2O \rightarrow OH+H$	919i	0.78 (0.71)	7.94×10^{3} (3.6×10^{4})	0.58	6.38×10^{6}
$OH \rightarrow O+H$	1046i	1.51 (1.55)	1.16×10^{-4} (4.1×10^{-5})	1.03	6.22×10^{1}
$OH+OH \rightarrow H_2O+O$	909i	0.46 (0.78)	4.51×10^{7} (1.47×10^{4})	0.56	5.66×10^{6}
$CO+O \rightarrow CO_2$	207i	0.68 (0.60)	8.25×10^{4} (5.58×10^{5})	1.17	1.25×10^{-2}
$CO+OH \rightarrow$ *cis*-COOH	224i	0.84 (0.46)	1.78×10^{4} (2.33×10^{7})	0.24	2.12×10^{10}
cis-$COOH \rightarrow CO_2+H$	1395i	0.80 (1.10)	5.03×10^{4} (9.67×10^{1})	1.32	2.43×10^{-2}
cis-$COOH+OH \rightarrow CO_2 + H_2O$	248i	0.33 (0.55)	3.22×10^{8} (9.72×10^{6})	0.96	1.04×10^{-1}
$H+H \rightarrow H_{2(g)}$	649i	0.78 (0.80)	6.88×10^{4} (3.91×10^{4})	0.47	1.61×10^{7}

Figure 1.- Top (upper panel) and side view (bottom panel) of the 2×2×1 supercell used to represent the Cu(321) surface. Labels a, b, c, d, e and f refers to the hollow positions, whereas labels 1, 2, 3, 4 and 5 refers to the top positions

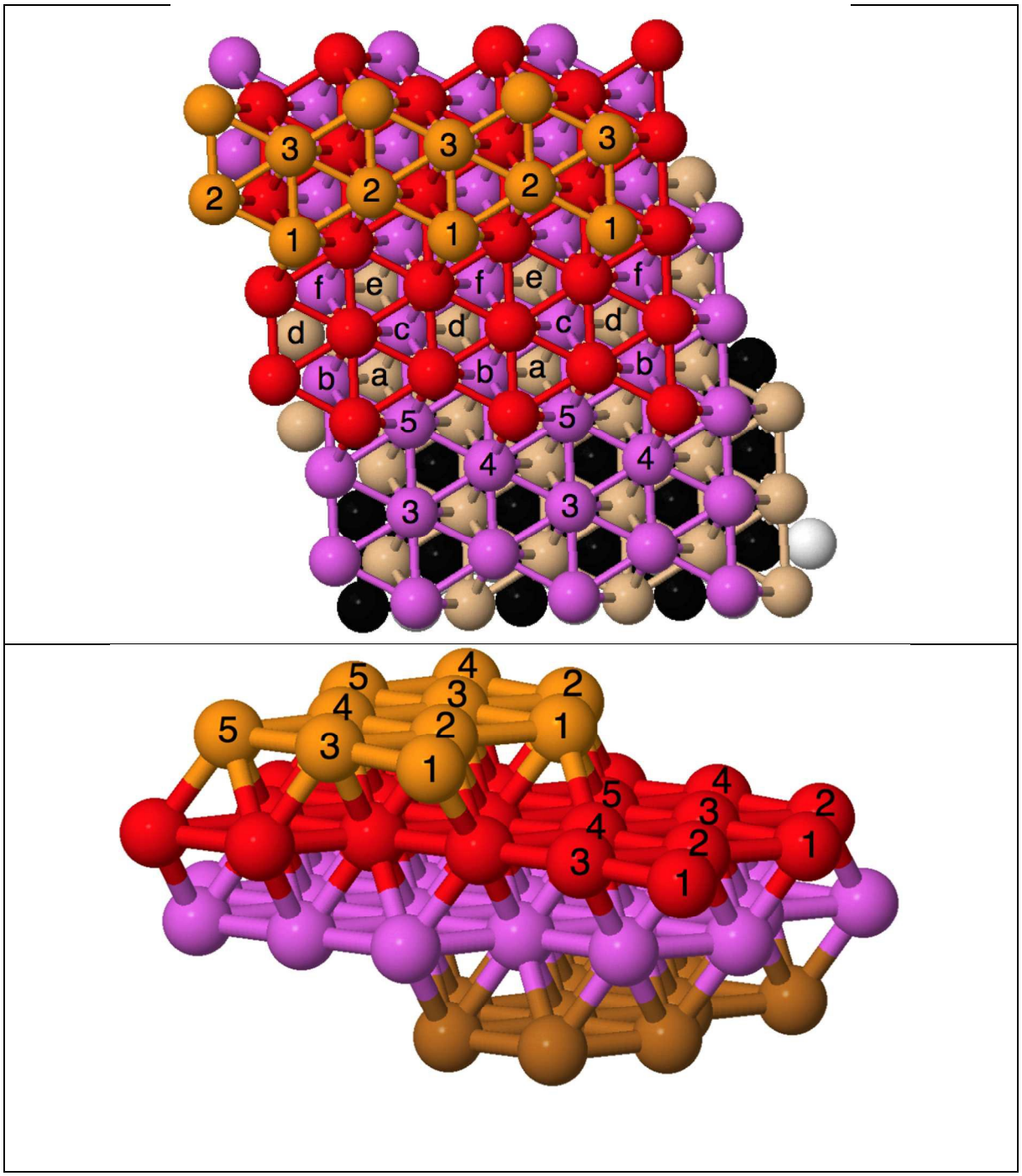

Figure 2.- Most stable configuration for H_2O (a), OH (b) CO (c), COOH (d), CO_2 (e) and H_2 (f) adsorbed species on the Cu(321) surface. Brown is used for Cu, grey for C, red for O and white for H. All the distances are in Å.

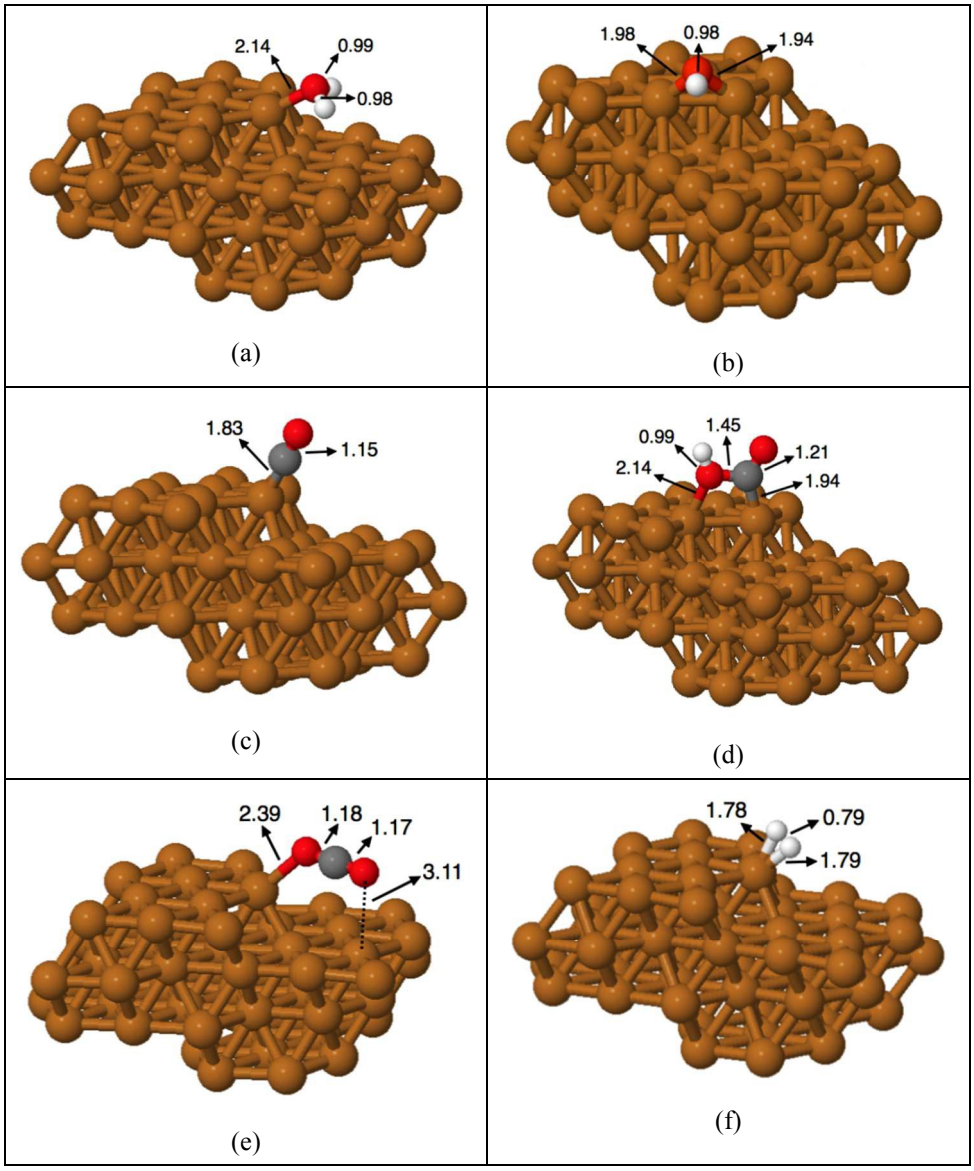

Figure 3.- Most stable configuration for OH+H (a), CO+OH (b), OH+OH (c), O+H (d), CO+O (e), H_2O+O (f), H+H (g), COOH+OH (h), CO_2+H (i) and CO_2+H_2O (j) co-adsorbed on the Cu(321) surface. Brown is used for Cu, grey for C, red for O and white for H. All the distances are given in Å.

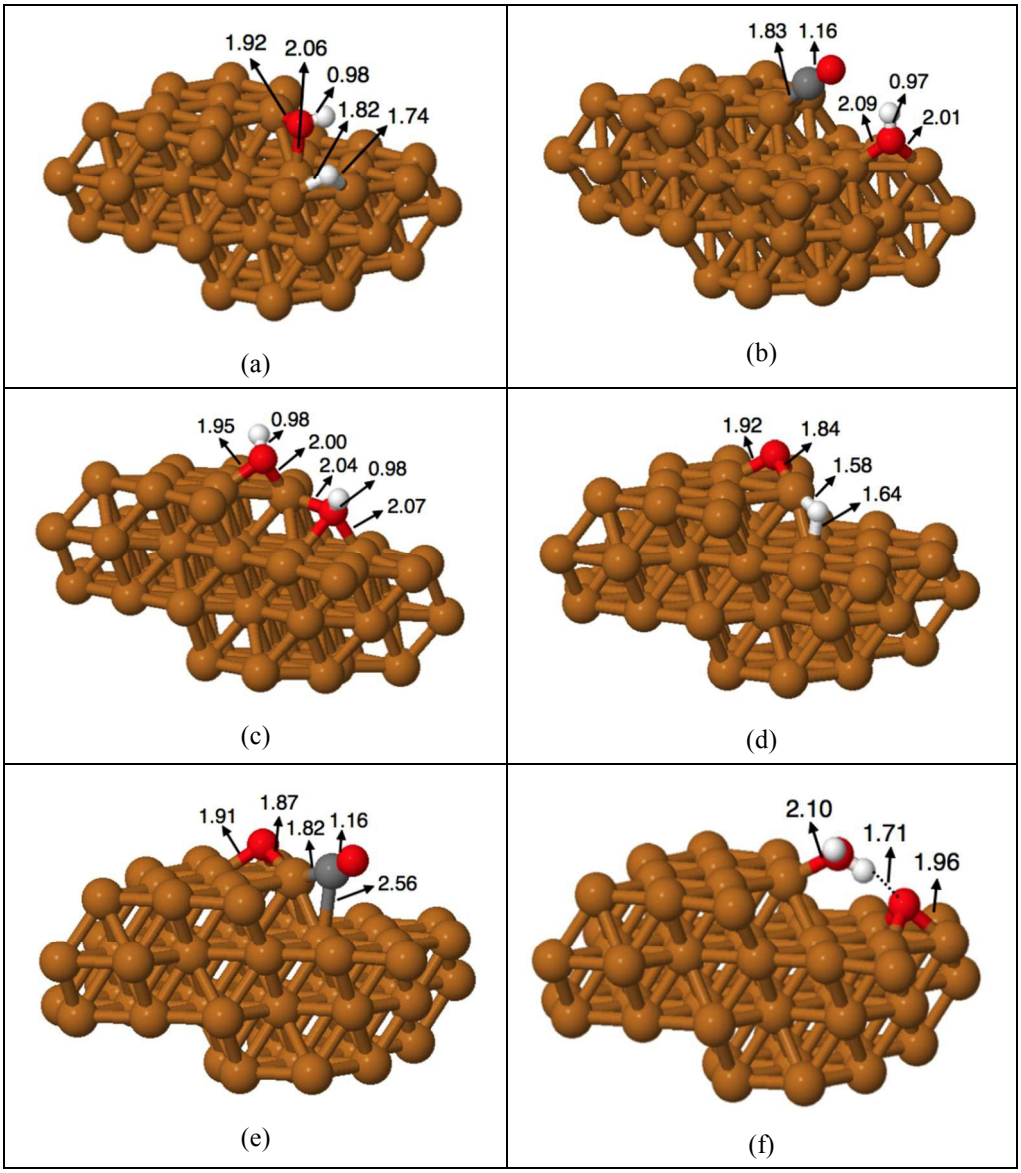

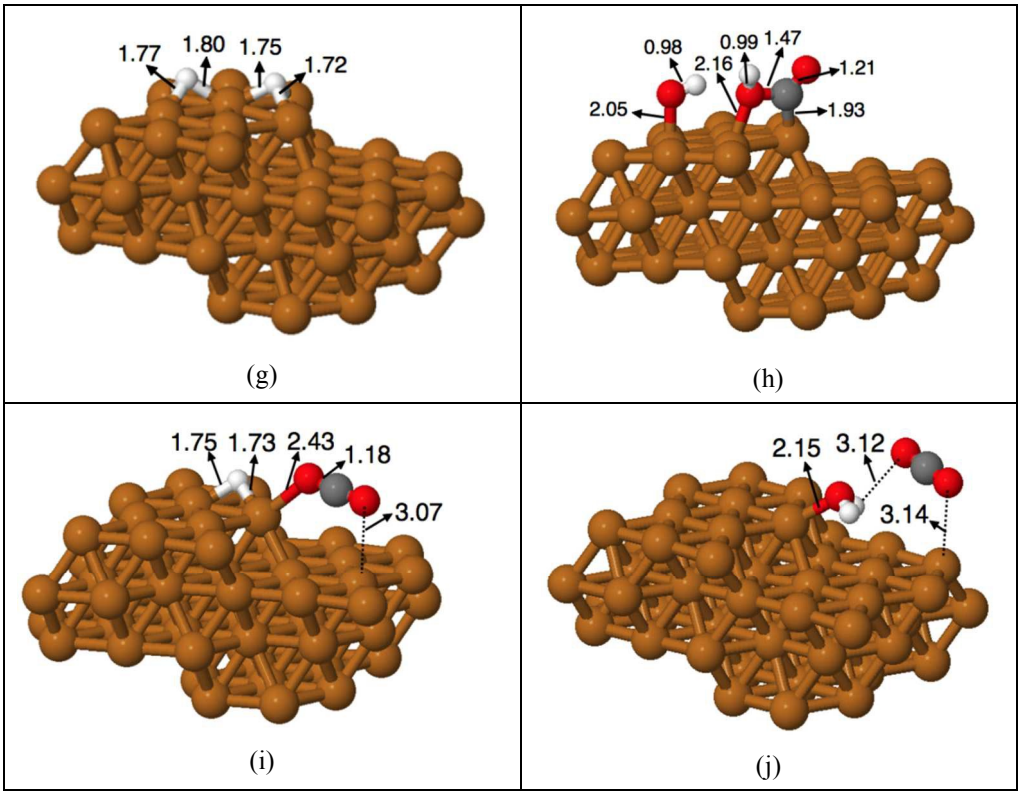

Figure 4 .- Schematic representation of the transition state structures for the $H_2O \rightarrow OH+H$ (a), $OH \rightarrow O+H$ (b), $OH+OH \rightarrow H_2O+O$ (c), $CO+O \rightarrow CO_2$ (d), $CO+OH \rightarrow COOH$ (e), $COOH \rightarrow CO_2+H$ (f), $COOH+OH \rightarrow CO_2+H_2O$ (g) $H+H \rightarrow H_2$ (h) elementary steps in Table 3 as obtained from PBE-D2 calculations. Brown is used for Cu, grey for C, red for O and white for H. All the distances are given in Å.

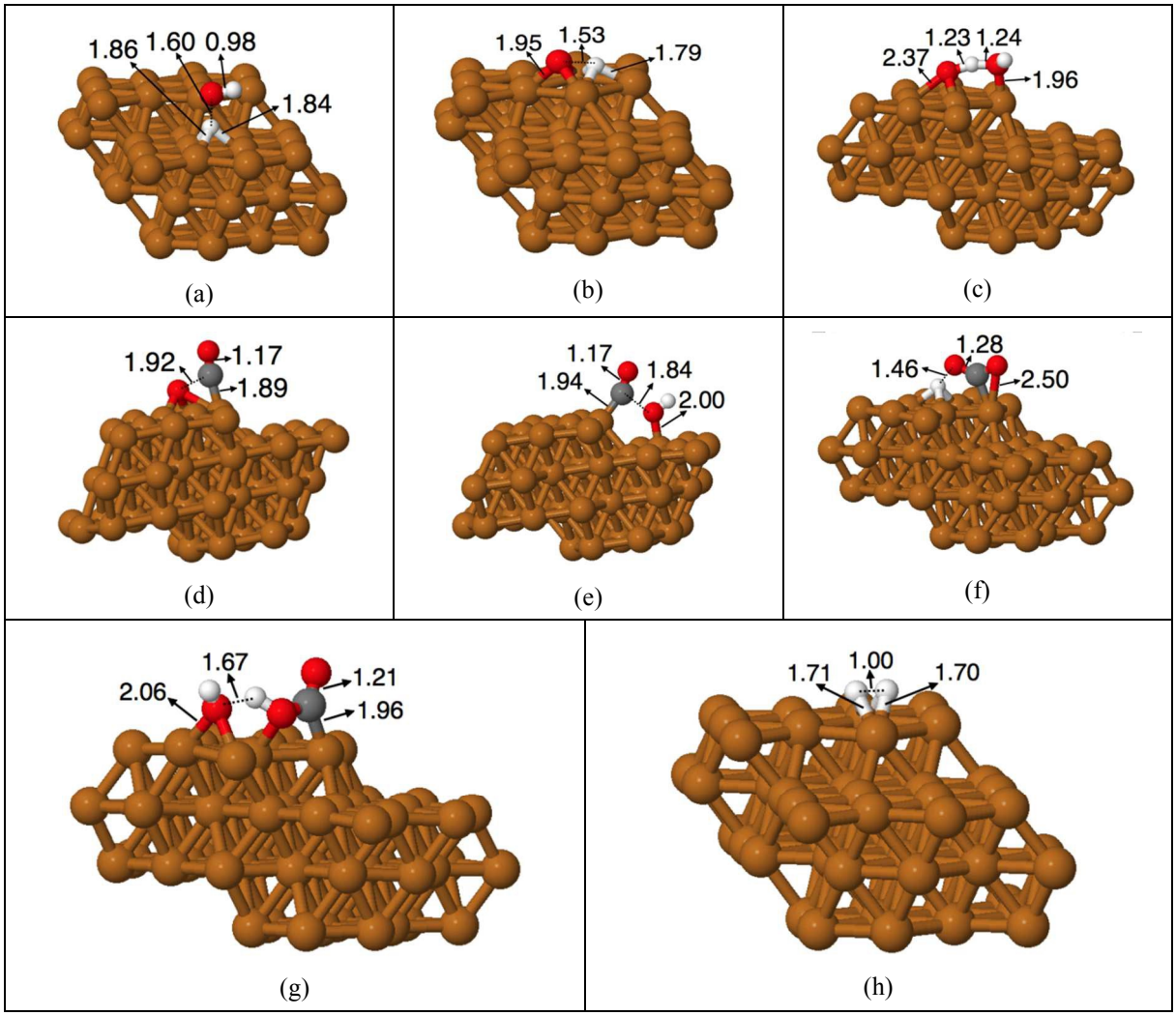

References

1 L. Grabow, W. Schneider, M. J Janik, T. Manz, A. van Duin, S. Sinnott and D. Scholl, *Computational Catalysis*, Royal Society of Chemistry Books, 2013.

2 J. K. Nørskov, F. Studt, F. Abild-Pedersen and T. Bligaard, *Fundamental Concepts in Heterogeneous Catalysis*, John Wiley & Sons, Inc., 2014, ISBN: 978-1-118-88895-7.

3 K. Reuter and M. Scheffler, *Phys. Rev. B,* 2002, **65**, 035406.

4 K. Honkala, K. Hellman, I. N. Remediakis, A. Logadottir, A. Carlsson, S. Dahl, C. H. Christensen and J. K. Nørskov, *Science*, 2005, **307**, 555-558.

5 J. K. Nørskov, T. Bligaard, J. Rossmeisl and C. H. Christensen, *Nature Chem.* 2009, **1**, 37-46.

6 J. K. Nørskov, F. Abild-Pedersen, F. Studt and T. Bligaard, *Proc. Natl. Acad. Sci. USA*, 2011, **108**, 937-943.

7 J. A. Dumesic, D. F. Rudd, L. L. Aparicio, J. E. Rekoske and A. A. Treviño, *The Microkinetics of Heterogeneous Catalysis*, American Chemical Society, Washington, DC, 1993**.**

8 A. A. Gokhale, A. J. Dumesic, M. Mavrikakis, *J. Am. Chem. Soc.* 2008, **130**, 1402-1414.

9 L. Yang, A. Karim, J. T. Muckerman, *J. Phys. Chem. C* 2013 **117**, 3414-3425.

10 H. Prats, L. Álvarez-Falcón, F. Illas, R. Sayos, *J. Catal.* 2016, **333**, 217-225.

11 Z. P. Liu, P. Hu, *J. Am. Chem. Soc.* 2003, **125**, 1958-1967.

12 S. Gonzalez, D. Loffreda, P. Sautet, F. Illas, *J. Phys. Chem. C* 2007, **111**, 11376-11383.

13 J. L. C. Fajín, M. N. D. S. Cordeiro, F. Illas, J. R. B. Gomes, *J. Cata*l. 2009, **268**, 131-141.

14 J. Rempel, J. Greeley, L. B. Hansen, O. H. Nielsen, J. K. Norskov, M. Mavrikakis, *J. Phys. Chem. C* 2009, **113**, 20623-20631.

15 J. L. C. Fajín, M. N. D. S. Cordeiro, J. R. B. Gomes, *J. Catal.* 2012, **289**, 11-20.

16 S. Lin, J. Y. Ma, L. S. Zhou, C. J. Huang, D. Q. Xie, H. Guo, *J. Phys. Chem. C* 2013, **117**, 451-459.

17 F. Viñes, J. R. B. Gomes, F. Illas, *Chem. Soc. Rev.* 2014, **43**, 4922-4939.

18 D. D. Langreth, M. J. Mehl, *Phys. Rev. B* 1983, **28**, 1809-1834.

19 J. P. Perdew, Y. Wang, *Phys. Rev. B* 1986, **33**, 8800-8802.

20 J. P. Perdew, Y. Wang, *Phys. Rev. B* 1992, **45**, 13244-13249.

21 J. P. Perdew, K. Burke, M. Ernzerhof, *Phys. Rev. Lett.* 1996, **77**, 3865-3868.

22 J. Janthon, S. M. Kozlov, F. Viñes, J. Limtrakul, F. Illas, *J. Chem. Theory Comput.* 2013, **9**, 1631-1640.

23 J. Janthon, S. J. Luo, S. M. Kozlov, F. Viñes, J. Limtrakul, D. G. Trulhar, F. Illas, *J. Chem. Theory Comput.* 2014, **10**, 3832-3839.

24 Y. Zhao, N. E. Schultz, D. G. Truhlar, *J. Chem. Theory Comput.* 2006, **2**, 364-382.

25 S. Kristyan, P. Pulay, *Chem. Phys. Lett.* 1995, **229**, 175-180.

26 A. D. Becke, *J. Chem. Phys.* 1993, **98**, 5648-5652.

27 R. Peverati, Y. Zhao, D. G. Truhlar, *J. Phys. Chem. Lett.* 2011, **2**, 1991-1997.

28 Y. Zhao, D. G. Truhlar, *J. Chem. Phys.* 2006, **125**, 194101.

29 R. Peverati, D. G. Truhlar, *Phys. Chem. Chem. Phys.* 2012, **14**, 13171.

30 N. E. Schultz, Y. Zhao, D. G. Truhlar, *J. Phys. Chem. A* 2005, **109**, 11127-11143.

31 J. N. Harvey, *Annu. Rep. Prog. Chem., Sect. C* 2006, **102**, 203-226.

32 N. E. Schultz, Y. Zhao, D. G. Truhlar, *J. Phys. Chem. A* 2005, **109**, 4388-4403.

33 S. F. Sousa, P. A. Fernandes, M. J. Ramos, *J. Phys. Chem. A* 2007, **111**, 10439-10452.

34 J. Paier, M. Marsman, K. Hummer, G. Kresse, I. C. Gerber, J. G. Ángyán, *J. Chem. Phys.* 2006, **124**, 154709(1-2).

35 C. H. Christensen, J. K. Nørskov, *J. Chem. Phys.* 2008, **128**, 182503(1-8).

36 P. Strasser, Q. Fan, M. Devenney, W. H. Weinberg, P. Liu, J. K. Nørskov, *J. Phys. Chem. B* 2003, **107**, 11013-11021.

37 S. Grimme, *J. Comput. Chem.* 2004, **25**, 1463-1473.

38 S. Grimme, *J. Comput. Chem.* 2006, **27**, 1787-1799.

39 S. Grimme, J. Antony, S. Ehrlich, H. Krieg, *J. Chem. Phys.* 2010**, 132**, 154104(1-19).

40 J. Klimes, A. Michaelides, *J. Chem. Phys.* 2012, **137**, 120901(1-12).

41 S. Grimme, *Comput. Mol. Sci.* 2011, **2**, 211-228.

42 P. G. Moses, J. J. Mortensen, B. I. Lundqvist, J. K. Nørskov, *J. Chem. Phys.* 2009, **130**, 104709(1-6).

43 B. A. De Moor, M. F. Reyniers, M. Sierka, J. Sauer, G. B. Marin, *J. Phys. Chem. C,* 2008, **112**, 11796-11812.

44 P. Janthon, F. Viñes, S. M. Kozlov, J. Limtrakul, F. Illas, *J. Chem. Phys.* 2013, **138**, 244701(1-8).

45 J. P. P. Ramalho, J. R. B. Gomes, F. Illas, *RSC Adv.* 2013, **3**, 13085-13100.

46 D. S. Newsome, *Catal. Rev. Sci. Eng.* 1980, **21**, 275-318.

47 N. Schumacher, A. Boisen, S. Dahl, A. A. Gokhale, S. Kandoi, L. C. Grabow, J. A. Dumesic, M. Mavrikakis, I. Chorkendorff, *J. Catal.* 2005, **229**, 265-275.

48 A. Bruix, J. A. Rodriguez, P. J. Ramírez, S. D. Senanayake, J. Evans, J. B. Park, D. Stacchiola, P. Liu, J. Hrbek, F. Illas, *J. Am. Chem. Soc.* 2012, **134**, 8968-8974.

49 J. A. Rodriguez, P. J. Ramírez, G. G. Asara, F. Viñes, J. Evans, P. Liu, J. M. Ricart, F. Illas. *Angew. Chem. Int. Ed*., 2014, **53**, 11270-11274.

50 *CRC Handbook of Chemistry and Physics*, 88th ed., Lide, D.R. (Ed.), CRC Press, Boca Raton, USA 2008.

51 Materials Studio Version 8.0, Accelrys Software Inc., San Diego.

52 G. Kresse, J. Hafner, *Phys. Rev. B*, 1993, **47**, 558-561.

53 G. Kresse, J. Furthmüller, *Comput. Mater. Sci.* 1996, **6**, 15-50.

54 G. Kresse, J. Furthmüller, *Phys. Rev. B* 1996, **54**, 11169-11186.

55 A. Tkatchenko, R. A. Di Stasio, R. Car, M. Scheffler, *Phys. Rev. Lett*. 2012, **108**, 236402(1-5).

56 J. L. C. Fajín, F. Illas, J. R. B. Gomes, *J. Chem. Phys.* 2009, **130**, 224702(1-8).

57 P. E. Blöchl, *Phys. Rev. B* 1994, **50**, 17953-17979.

58 G. Kresse, D. Joubert, *Phys. Rev. B* 1999, **59**, 1758-1775.

59 H. J. Monkhorst, J. D. Pack, *Phys. Rev. B* 1976, **13**, 5188-5192.

60 J. L. C. Fajín, M. N. D. S. Cordeiro, J. R. B. Gomes, F. Illas, *J. Chem. Theory and Comput.* 2012, **8**, 1737-1743.

61 A. Heyden, A. T. Bell, F. J. Keil, *J. Chem. Phys.* 2005, **123**, 224101(1-14).

62 M. P. Andersson, *J. Theo. Chem.* 2013, **2013**, 327839.

Graphic for TOC